

Simple Modeling and Prototype Experiments for a New High-Thrust, Low-Speed Permanent Magnet Disk Motor

Genevieve Patterson^{1*}, Takafumi Koseki¹, Yasuaki Aoyama², Kentaro Sako¹

¹Department of Electrical Engineering and Information Systems, The University of Tokyo, Tokyo, Japan

²Hitachi Research Laboratory, Hitachi, Ltd., Ibaraki-ken, Japan

E-mail: Patterson.genevieve@gmail.com

Abstract--Fully integrated electric propulsion systems are gaining popularity in both commercial and military sectors. Propulsion motor manufacturers are investigating new direct drive solutions for use in electric ships. These applications require motors with high torque output at low speeds. Such requirements were the motivation for the design of a new PMSM with a novel topology.

This paper describes the efficient mathematical model used to optimize our PMSM design. Based on a simplified theoretical model for the motor's behavior, we were able to quickly and accurately predict torque output. The minimalist design of this TFM is shown to be advantageous for computer simulation and machine manufacturing. Initial results from a prototype are included and discussed. Future plans for the prototype are outlined.

Index Terms— electric propulsion, permanent magnet synchronous motor (PMSM), transverse flux machine (TFM), tunnel actuator (TA)

I. INTRODUCTION

Just as the commercial automotive, aerospace, and railway industries have been affected by rising fuel costs, the marine industry has recently endeavored to create more fuel-efficient, cost-effective drive systems. During the last 15-20 years, fully electrified propulsion (EP) systems have been gaining popularity and capturing most of the market growth in sectors such as cruise ships, passenger ferries, oil and gas transport vessels, and merchant and special order ships [1,2]. The popularity of EP is due to savings in onboard space, fuel, electrical losses, noise and vibrations, and maintenance.

Several different types of motors are currently in use or have been proposed for application in ship propulsion. We took particular interest in a PMSM solution because of the possibility of higher thrust, less complicated design, and lower maintenance when compared with induction motor solutions. PMSMs are also much less expensive than high temperature superconductor machines.

Due to the short pole pitch characteristic of certain types of PMSM designs, these machines can have high torque at low speeds, which is particularly beneficial in a marine application. Transverse flux motor designs have short pole pitch and high torque characteristics, but TFMs are plagued by low power factor [3]. In order to improve on previous designs, we developed a theoretical model of a transverse flux PMSM and subsequently built and tested the prototype of a new design. We also adapted the

basic flux path idea present in the Tunnel Actuator, a linear PMSM produced by Hitachi, to perform in a rotary application.

II. FUNDAMENTALS OF THE NEW MOTOR DESIGN

The transverse flux machine takes advantage of a 3-D flux path to increase torque production without having to trade off between electrical or magnetic loading as with radial and axial flux machines. But the TFM described by Weh, et. al. and later improvements on that design have such complex manufacturing requirements that they are impractical for industrial production [4]. This complex design can be seen in Fig.1. Ultimately, the low power factor characteristic of transverse flux machines becomes an obstacle against this type of machine attaining a high real power to volume ratio [3]. For example, Rolls-Royce Ltd. manufactured a TFM for marine propulsion that was capable of large thrust but had power factor ratings of less than 0.7 [6].

When examining the field of direct drives for another motor with a similar flux path configuration but a high power factor, we found Hitachi's Tunnel Actuator, now available commercially as the H type Motor, for linear drive applications [5]. This drive has the advantages of easy assembly, thin permanent magnet and high resultant permeability, and a magnetic flux path that is transverse. The TA suffered from large leakage flux due to the close position of the armature poles and the configuration of the flux path in alternating poles. We thought that by placing only poles with flux in the same direction next to each other and spacing them further apart to increase magnetic isolation, we could create a better design. The following sections will show the details of our new direct drive design.

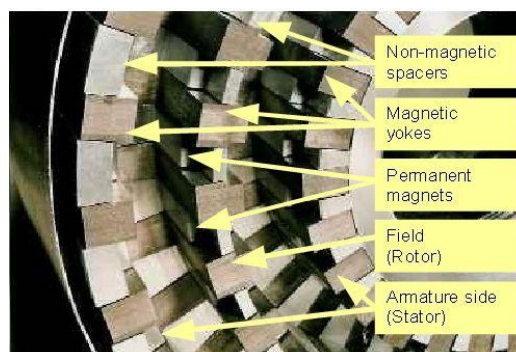


Fig. 1. Transverse Flux Machine

A. One Pole Model

The theoretical model for our machine was created by breaking down a transverse flux PMSM into its fundamental components. The basic unit of the model was one pole of the machine. A whole motor would have n poles per phase and m number of phases.

One pole consists of a stator C-core, where an air gap makes the break in the 'C'. The winding is wrapped around the back of the C, and the permanent magnets on the rotor are accelerated through the air gap to generate thrust. An illustration of the one-pole model is in Fig. 2. The input to the model is the armature current I_a . B_a is the armature flux, and B_f is the flux contributed by the field magnets. As I_a changes, the polarity of B_a also fluctuates, which pulls the alternating polarity magnets through the air gap, creating thrust. The movement of the magnets through the armature flux field also induces an internal EMF.

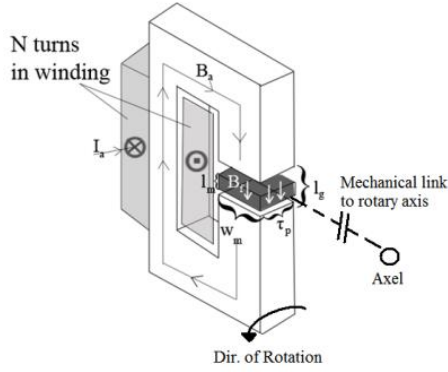


Fig. 2. One-Pole Model Diagram

Fig. 3 shows how the rotor would be propelled through the consecutive air gaps of several poles connected in phase by their armature winding. The self-induced voltage and thrust contributed by each pole would be superimposed to create the total contribution of one phase. The phases of the machine could then be connected to the operator's convenience. The C-cores of each phase would be placed at balanced angular separation around the axle to create the outer radius of the machine. An illustration of a full version of the machine is shown in Fig. 7.

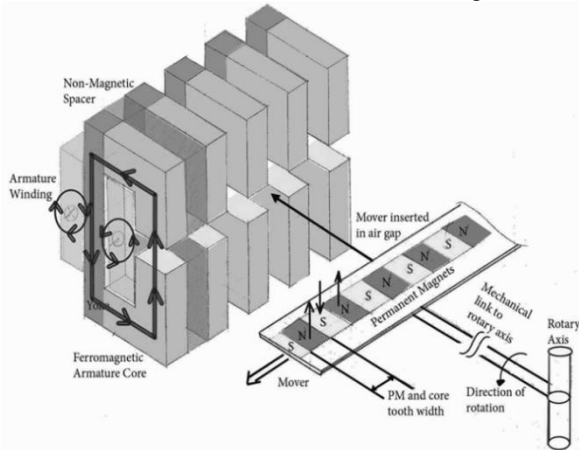


Fig. 3. Flux Path through C-Core and Rotor

B. Per Phase Quasi-Stationary Equivalent Circuit Models

Fig. 4 shows the per phase equivalent circuit for a 3-phase machine composed of n connected C-cores. L_s and R_s are the synchronous armature inductance and resistance, respectively, but for the sake of simplicity R_s is ignored in the following calculations. V_0 is the induced EMF, and V_a the armature voltage.

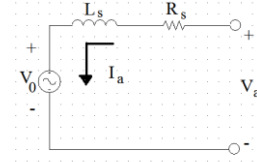


Fig. 4. Per Phase Equivalent Circuit Model

Assuming that the motor has a n number of poles per phase and a three-phase star connection, Eqns. 1-6 show how the armature voltage V_a , the synchronous impedance voltage drop V_s and the self-induced voltage V_0 are calculated. The per phase armature self-inductance L_a and 3-phase synchronous inductance L_s , are inversely proportional to the air gap length l_g as shown in Eqns. 2-4. L_s is twice L_a because there are two stator poles per phase. This model neglects lossy elements because low losses are expected due to the magnetic isolation of the separate C-cores.

$$V = R_s * I_a + L_s \frac{dI_a(t)}{dt} + V_0 \quad (1)$$

$$V_s = L_s \omega_e I_a \quad (2)$$

$$L_s = 2 * L_a \quad (3)$$

$$L_a = N^2 / R \quad (4)$$

$$R = \frac{l_g}{\mu_0 S} \quad (5)$$

$$V_0 = \frac{3}{2} \beta S N B_f \omega_e \quad (6)$$

$$\Phi_f = \frac{H_c * l_m}{R_{magnet}} \quad (7)$$

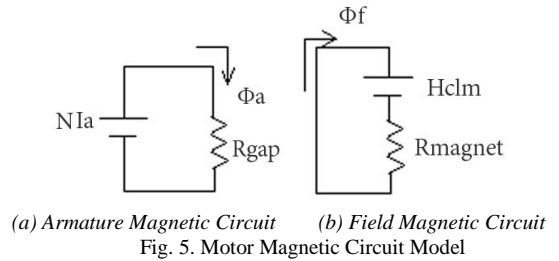
$$\Phi_a = \frac{N I_a}{R_{gap}} \quad (8)$$

$$\Phi_{total} = \Phi_a + \Phi_f \quad (9)$$

$$B_f = \frac{\Phi_f}{S} \quad (10)$$

$$B_a = \frac{\Phi_a}{S} \quad (11)$$

$$F = \frac{3}{2} \beta B_a H_c l_m w_m \quad (12)$$



(a) Armature Magnetic Circuit (b) Field Magnetic Circuit
Fig. 5. Motor Magnetic Circuit Model

In Eqns. 4-6 S is the surface area of the PM and ω_e the synchronous angular speed. β is a form factor for matching the realistically jagged V_0 signal to a fundamental frequency. Eqn. 10 determines the PM flux density, which depends inversely on the magnet

reluctance. Eqn. 11 determines the armature flux density, and B_a has the same inverse proportionality to air gap reluctance.

This mathematical model is predicated on the idea of superposition. The magnetic flux, flux linkage, and induced voltage are all calculated for the unit core. The value for the whole machine is later calculated as multiple of the cores per phase and the number of phases in the motor. The total magnetic flux present in a single unit loop is also calculated as the superposition of the flux due to the armature winding plus the flux due to the permanent magnet.

Fig. 5 illustrates how the magnetic circuit model uses superposition. We chose to model the magnetic circuits as seen from the armature and field perspectives separately. The total magnetic flux is then a summation of the flux due to the armature winding and that due to the field magnet. Refer to Eqns. 7-9 for a mathematical description of this relationship.

A difficulty arises in this superposition, though. When the permanent magnet is not perfectly aligned with the ferromagnetic core, it does not contribute its full flux capability to the total flux value. This model treats the permanent magnet as a virtual coreless coil that can be divided easily without effecting the basic physical equations.

Eqn. 12 shows the thrust force produced by the whole three-phase machine. If the mechanical clearance, the space in the air gap not occupied by the magnet, is a value significantly smaller than l_m , then l_m and l_g are approximately the same. Thus, increasing l_m while keeping all other factors constant will not significantly increase thrust. The whole volume of the magnet is effectively controlled by $l_m w_m$ because the pole pitch must remain a constant value for a given input frequency. Magnet volume or its excitation strength, indicated by H_c , must increase in order to raise F . Eqns. 7 and 8 indicate that if a larger mechanical clearance is necessary then the designer must accept lower flux density.

C. Power Factor and Thrust Calculation

In order to determine the power factor for the basic unit model, Fig. 6 shows the phasor diagram for the 3-phase configuration's synthesized voltage vectors. In Fig. 6 the angles ϕ_{Ra} and ϕ are the power factor angles considering armature resistance and disregarding it, respectively. The value of ϕ_{Ra} would always be smaller than ϕ regardless of the value of the armature resistance, thus real-world PF values may be slightly better than those estimated by the model in this paper. Future research will likely include consideration of R_a .

Eqns. 13 and 14 show how the power factor and power factor angle are calculated. It is important to note that ϕ is not dependent on the input frequency, as shown in Eqn. 14. This indicates that ω_e can be increased, which increases the output thrust, but the power factor will remain the same. The absolute values of the internal voltages will however increase.

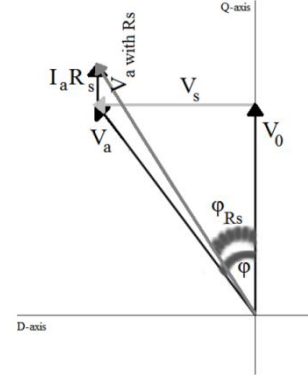


Fig. 6. Phasor Diagram for Symmetrical 3-phase Machine

$$p.f. = \cos \phi \quad (13)$$

$$\tan \phi = \frac{V_s}{V_0} = \frac{3 \mu_0 N I_a}{2 \beta H_c l_m} = \frac{l_g F}{\beta H_c^2 l_m^2 w_m} \quad (14)$$

$$I_a = \frac{2 l_g F}{3 N \mu_0 H_c l_m w_m} \quad (15)$$

Assuming $l_g \cong l_m$

$$\text{Then, } \tan \phi = \frac{F}{\beta H_c^2 l_m w_m} \quad (16)$$

Using the expression for I_a in Eqn. 15, the formula in Eqn. 16 illustrates the relationship between the power factor angle and thrust. If the volume and strength of the magnet are constant, when thrust F raises the power factor lessens. The model verifies that there is an unavoidable tradeoff between power factor and thrust when the permanent magnet excitation is constant.

III. CREATION OF THE PROTOTYPE AND TEST BENCH

The prototype design was created by taking a number of unit model C-cores and arranging them radially to create a full stator. In Fig. 7 this idea is drawn up with 3-phases and 4 stator cores per phase. In the actual prototype, only 2 cores were used per phase. The rotor was constructed in a similar fashion by placing alternating polarity magnets on a rotor backing at a set angular separation. In the prototype there were 36 PMs, thus 18 pole pairs.

It is important to note that because the flux lines in adjacent stator cores of the same phase point in the same direction and there is a large physical separation between phases, we expected negligible leakage flux.

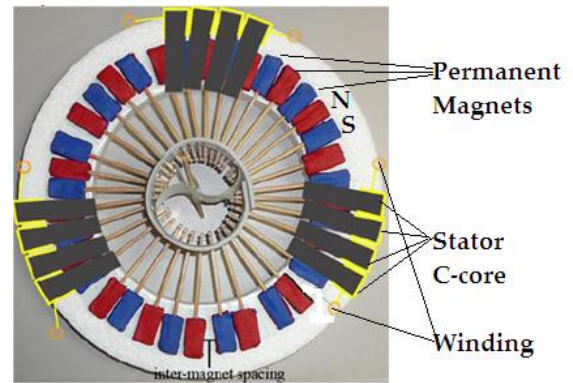


Fig. 7. Illustration of Rotary Disk Motor Design Concept

Fig. 8 is a photograph of the actual prototype. It was observed during the set-up of this prototype that the precise positioning of the stator cores was significant. As previously mentioned, one of the fundamentals of the mathematical model was that the flux contribution from each C-core could be simply added by super position. This assumption fails if the stator cores are not perfectly in phase. The in-phase position of the stator cores needs to be more precise the closer together the rotor magnets are, and because this was a small scale prototype the acceptable positioning error was quite small.

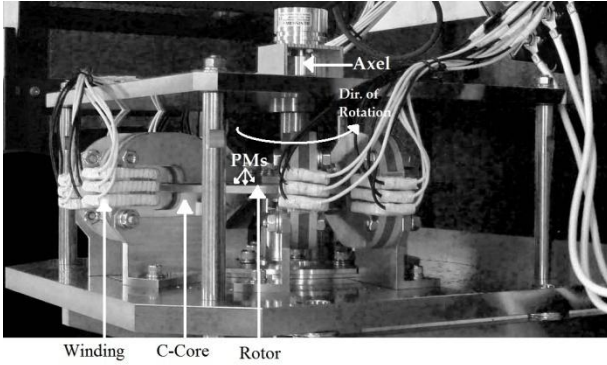


Fig. 8. Prototype Motor

The full test bench involved directly connecting a PMSM load motor to the prototype. The prototype was driven directly in generator mode during the open circuit testing in Section IV. The prototype was connected to an inverter to be controlled for dynamic testing. This test bench accurately represents the typical case of an industrial client, where the motor supplier will have only general knowledge about the loading conditions applied to their product.

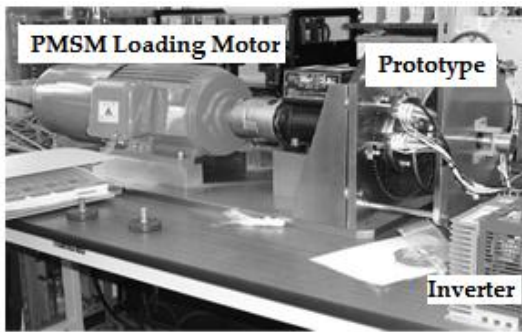


Fig. 9. Prototype Test Bench

IV. NO LOAD AND QUASI-STATIONARY TESTING

There were two phases to the machine characterization testing. These two tests will be outline in the subsequent sections.

A. Open Circuit Test

Firstly, the open circuit voltage was measured. This test is crucial for identifying internal reversed electromotive force as a function of speed. This characteristic is used to calculate the motor constant used in the speed controller. The motor constant is the most significant performance index of the motor.

Figure 10 show the test circuit for this stage. The ‘Ch 1’ reference shows how this circuit was connected to the scope. V_0 represents the back EMF.

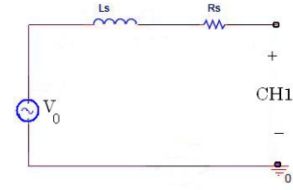


Fig. 10. Open Circuit Test Circuit with Oscilloscope Connection Label

During testing, the prototype’s most stable operating range was at approximately 50Hz input frequency. Figure 11 demonstrates that the empirical values for V_0 at this speed are slightly less than the theoretical calculations. This is a reasonable expectation because the theoretical V_0 was calculated using the maximum flux density possible in the air gap. This peak value is less in reality because the flux output is forced to approximate a sinusoidal waveform.

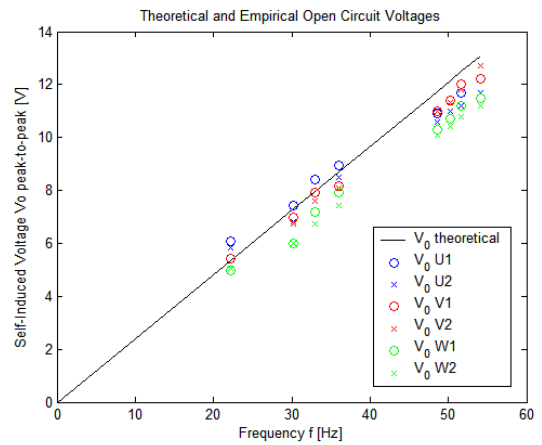


Fig. 11. Per Pole Open Circuit Voltage

B. Stationary Rotor Direct and Quadrature Axis Armature Inductance Test

The stationary armature impedance test was completed in order to identify the real and imaginary internal synchronous impedances. A DC test to measure the armature resistance and an adaptation of the short circuit test commonly described in electromechanical machine literature would be optional to confirm the results of this test.

The test circuit is given in Fig. 12.

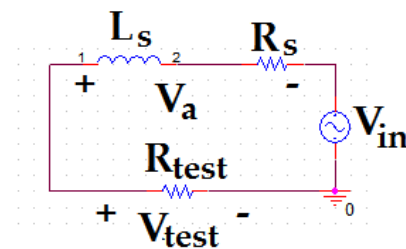


Fig. 12. Stationary AC Input Armature Impedance Test Circuit

$$Z_s = \frac{V_a e^{i\theta}}{V_{test}/R_{test}} \quad (17)$$

$$\theta = 2 * \pi * \tau / T \quad (18)$$

$$Z_s = R_s + j * \omega * L_s \quad (19)$$

The open layout of the prototype made it possible to observe if the rotor was stopped with the PM aligned with the stator core (d-axis) or 90° out of alignment (q-axis). Figures 13 and 14 show the complex impedance vector at different frequencies. It is significant that the real axis values for each vector, the armature resistance value, is close to 0.43Ω for each vector in both the d-axis and q-axis cases, although the q-axis values are slightly more.

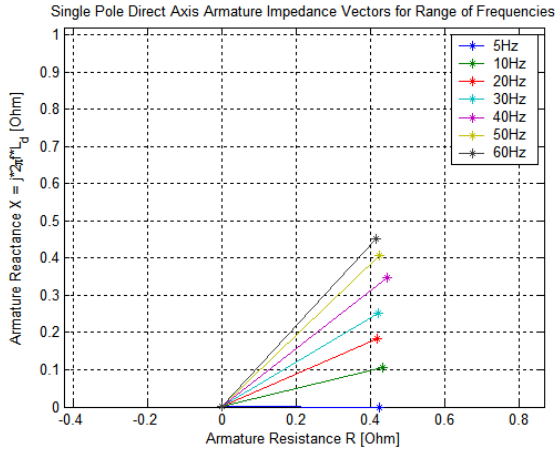


Fig. 13. Per Pole Direct Axis Complex Impedance Vectors for a Range of Input Frequencies

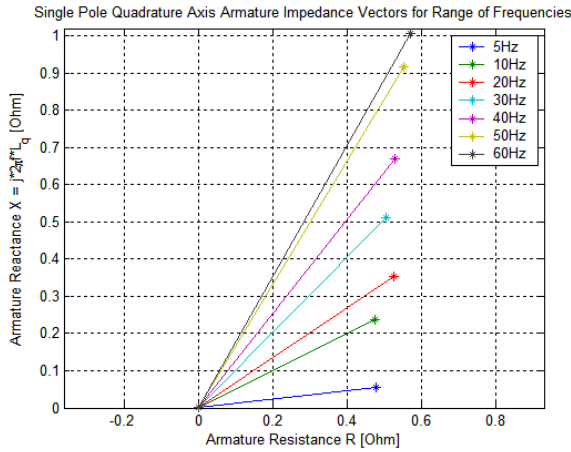


Fig. 14. Per Pole Quadrature Axis Complex Impedance Vectors for a Range of Input Frequencies

Figure 15 compares the theoretical and empirical values for armature inductance per pole. Eqns. 3 and 4 show how the theoretical values were calculated, except that for the q-axis value 10 times the permeability of free space was assumed for the rotor backing material. At the motor's stable operating frequency, the values for L_d and L_q are almost constant and within theoretical limits.

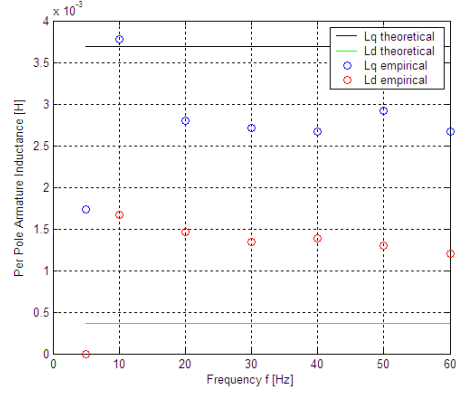


Fig. 15. Per Pole Direct Axis Complex Impedance Vectors for a Range of Input Frequencies

V. SPEED CONTROL AND DYNAMIC PERFORMANCE EXPECTATIONS

A. Speed and Current Controller

The speed controller designed for the prototype was a conventional cascade controller using the parameters calculated in the last section for the motor's plant model. There were three steps in the construction of this controller. The first was the 3-phase AC input to 2-phase direct/quadrature input transformation. The second step was to make a PI controller with feed-forward EMF compensation. The third part was a PI speed controller for suppressing the effects of load torque. C. Kessler's canonical form was used to calculate the PI gains. The motor constant was calculated from the open circuit test.

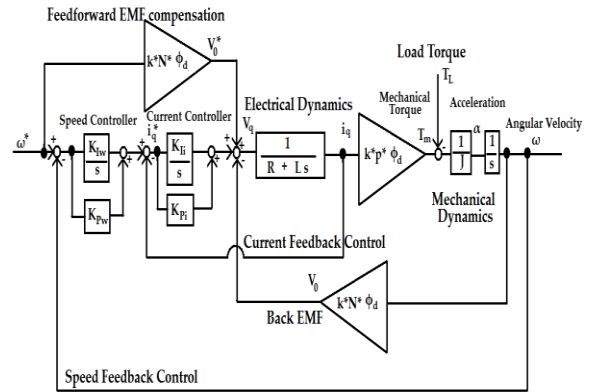


Fig. 16. Cascaded PI Speed Controller and Q-Axis Current Controller

Fig. 16 shows the outline of the controller without the 3-phase to 2-phase transformation. This model assumes that the motor is non-salient pole and $I_d = 0$. Thus only the Q-axis relationships are shown in Fig. 16.

B. Planned Dynamic Testing and Anticipated Results

Table I shows the theoretical and empirical values for the efficiency, power factor, torque, and force density of the prototype. Due to the agreement of the simulated values for V_0 and Z_s , the expectation is that the dynamic behavior will also match predictions. The torque and force density are high for this type of machine, and thus

the results are encouraging. The tradeoff between torque and power factor are also made obvious. The operating point of 50 Hz was selected because that is the typical operating frequency of electric ships.

TABLE I
COMPARISON OF THEORETICAL AND EMPIRICAL DATA

Variable	Theoretical Value	Empirical Value
frequency	50 Hz	50 Hz
N	84	84
$L_s=2*(L_d+L_q)/2$	4.16 mH	3.86 mH
R_s	0.75 Ω	0.75 Ω
I_a	4 A	4 A
V_0	9.78 V RMS	14.85 V RMS
V_a	14.04 V RMS	18.88 V RMS
Φ_f	5.24×10^{-4} Wb	7.96×10^{-4} Wb
B_f	0.44 T	0.66 T
B_a	4.98×10^{-4} T	4.98×10^{-4} T*
PF	0.93	0.97*
η	0.70	0.79*
$P_{mechanical}$	117.38 W	178.19 W*
Torque	6.73 Nm	10.21 Nm*
Force Density	$50 \text{ kN/m}^2 = 0.49 \text{ atm}$	$75.6 \text{ kN/m}^2 = 0.75 \text{ atm}^*$

*values are estimated based on empirical values for V_0 and Z_s

The data from Table I is encouraging because of the high thrust and power factor. It is expected that by increasing the armature winding number it would be possible to improve the efficiency in later prototypes.

VI. CONCLUSION

This paper proposed a new evolution in the development of the transverse flux type permanent magnet motor. A new idea for a low-speed, high-torque permanent magnet motor was proposed. We reviewed the initial transverse flux concept and two adaptations of the TFM topology. The concept outlined by Husband and Hodge in [6] gave encouraging results about the possibility of applying a direct drive solution to electric ship propulsion, but presented difficulties in the complexity of manufacturing and in a low power factor characteristic.

The new design introduced in this paper re-imagines the transverse flux path. It has a simple flux topology that allowed for simplified linear modeling of the motor characteristics. The fundamental stationary characteristics of the new motor design were estimated analytically based on an elementary magnetic circuit analysis.

In the process of developing the mathematical model for this motor, the unavoidable tradeoff between thrust and power factor in a TFM was confronted. The linearity of our model allowed for a direct examination of this compromise that has been observed in the literature of TFM development.

In Section III the original plan for a prototype was presented. Although the layout of the machine and test bench lent itself well to rapid construction and direct measurement techniques, the placement of the stator cores had to be carefully planned to prevent torque ripple. The angular positioning of the C-cores was the most

significant step in preparing the prototype for stationary and running tests.

The fundamental measurements of the prototype's open circuit voltage and armature impedance were completed successfully in Section IV. The results of these measurements verified the accuracy of the mathematical model presented in Section II. The prognosis of these motor parameters contributed to the speed controller design for the prototype motor.

At the time of publication, the plan for future work on this project is clear. Dynamic testing must be conducted to verify the expectations presented in Section V. The next step we will take is to propose an improvement to the initial design in order to reduce the possibility of torque ripple and increase the ease of assembly. The results of dynamic testing and future prototype design may be presented at the time of the conference.

ACKNOWLEDGMENT

We would like to thank the Hitachi Research Laboratory for their technical advice in support of this research. We are also grateful to the Japan Society for the Promotion of Science for their partial financial support of this project through the 2009 Grant-in-Aid for Scientific Research© program.

REFERENCES

- [1] Borman, J., Sharman, B., "Electric Propulsion of Passenger Ships and Other Vessels," *Trans. ImarE*, pp. 77-104, 16 Nov. 1993.
- [2] ABB, "ABB Marine – References," www.abb.com/marine, Center of Excellence Cruise & Ferries: ABB Oy, Helsinki, Finland, December 2006.
- [3] Harris, M.R., Pajooman, G.H., Abu Sharkh, S.M., "The Problem of Power Factor in VRPM(Transverse-Flux) Machines," *IEEE Conference on Electrical Machines and Drives 1997*, Publication No. 444, IEEE, Sept. 1997.
- [4] Weh, H., Hoffman, H., Landrath, J., "New Permanent Magnet Excited Synchronous Machine with High Efficiency at Low Speeds," *Proceedings of the International Conference on Electrical Machines*, 1988.
- [5] Kim, HJ, Nakatsugawa, J, Sakai, K, Shibata, H, "High-Acceleration Linear Motor, 'Tunnel Actuator,'" *The Magnetics Society of Japan*, Vol. 29, No. 3, pp 199-204, 2005.
- [6] Husband, S.M., Hodge, C.G., "The Rolls-Royce Transverse Flux Motor Development," *Electric Machines and Drives Conference*, Vol. 3, pp. 1435-1440, IEEE, 2003.